Effect of freezing prior to X-ray micro computed tomography on the microstructure of a highly decomposed peat material close to water saturation

Hassan Al Majou[1,2], Ary Bruand[1], Olivier Rozenbaum[1,3], Emmanuel Le Trong[1]

[1] Université d'Orléans, CNRS, BRGM, Institut des Sciences de la Terre d'Orléans (ISTO), 1A rue de la Férollerie, 45071 Orléans Cedex 2 (France)

[2] University of Damas, Department of Soil Science, Faculty of Agronomy, PO Box 30621, Damas (Syria)

[3] CNRS, Conditions Extrêmes et Matériaux : Haute Température et Irradiation (CEMHTI), UPR 3079, 1 Avenue de la Recherche Scientifique, 45071 Orléans, Cedex 2 (France)

Correspondence to: Ary Bruand (Ary.Bruand@univ-orleans.fr)

Abstract. The modelling of peatland functioning, in particular the impact of anthropogenic warming and direct human disturbance on CO_2, CH_4 and N_2O, requires detailed knowledge of the peat structure and of both water and gas flow with respect to the groundwater table level. To this end, freezing is nowadays increasingly used to obtain small size peat samples for X-ray micro computed tomography (X-ray µ-CT) as required by the need to increase the resolution of the 3D X-ray CT images of the peat structure recorded. The aim of this study was to analyze the structure of a peat material before freezing and post-defreezing using X-ray µ-CT and to look for possible alterations in the structure by analyzing the air-filled porosity. A highly decomposed peat material close to water saturation was selected for study and collected between 25 and 40 cm depth. Two samples 4×4×7 cm^3 in volume were analyzed before freezing and post-defreezing using an X-ray µ-CT Nanotom 180NF. Results showed that the continuity and cross section of the air-filled tubular pores several hundreds to about one thousand micrometers in diameter were altered post-defreezing. Many much smaller air-filled pores not detected before freezing were also recorded post-defreezing with 470 and 474 pores higher than one voxel in volume (60×60×60 μm^3 in volume each) before freezing, and 4792 and 4371 air-filled pores higher than one voxel in volume post-defreezing for the two samples studied. Detailed analysis showed that this increase resulted from a difference in the whole range of pore size studied and particularly from a dramatic increase in the number of air-filled pores ranging between 1 voxel (216 10^3 μm^3) and 50 voxels (10.8 10^6 μm^3) in volume. The increase in the specific volume of water by 8.7% when it turns from liquid to solid because of freezing led to the creation of a pore volume in the organic matrix which remained saturated by water when returning to room temperature. This induced the desaturation of some of the finest tubular pores as well as some the largest pores of the porous organic matrix which were both water-filled before freezing. The volume of these pores newly occupied by air using X-ray µ-CT and their total volume was found to be consistent with the one calculated as resulting from the increase in the specific volume of water when it turns into ice. They correspond to small air-filled pores several voxels in volume to several dozen voxels in volume and to discontinuous air-filled fine tubular pores which were both detected only post-defreezing. Finally,

the increase in the specific volume of water because of freezing and related increase in the porosity of the water-saturated porous matrix also appear also to be responsible for the alteration of the air-filled tubular pores detected before freezing as shown by the 3D binary images and the pore volume distribution.

1 Introduction

In many peatland studies, the description of peat physical characteristics is derived from only a few basic metrics such as porosity, bulk density and humification indexes (Michel et al., 2001; Quinton et al., 2009; Michel, 2015; Kurnain and Hayati, 2016). However, the short- and long-term modelling of peatland functioning, and in particular the impact of anthropogenic warming and direct human disturbance on atmospheric CO_2, CH_4 and N_2O, requires detailed knowledge of the peat structure and of both water and gas flow with respect to the groundwater table level (e.g. Gharedaghloo et al., 2018; Zhao et al., 2020; Glaser et al., 2021; Muller & Fortunat, 2021; Swinnen et al., 2021; Wiedeveld et al., 2021). To achieve this, X-ray Computed Tomography, which is widely used in science as a non-invasive technique for the study of internal 2D and 3D structures, is a promising technique to analyze the structure of peats and their physical properties. Improvements in resolution led to the development of X-ray micro computed tomography (X-ray μ-CT), which has been applied to peat materials. Kettridge and Binley (2008 and 2011) used X-ray μ-CT to investigate gas content and peat structure. They studied samples 7.2 cm long and 7.2 cm in diameter with a resolution of 100 μm. Quinton et al. (2009) analyzed the structure and hydraulic properties of peats using X-ray CT. They studied samples 10 cm long and 6 cm in diameter with a resolution of 45 μm and showed how water contents recorded in the field were related to the inter-particle pore volume distribution. Using the methodology developed by Quinton et al. (2009), Rezanezhad et al. (2009 and 2010) studied the influence of pore size geometry on peat unsaturated hydraulic conductivity by combining X-ray μ-CT and digital image processing. They found that the large reduction in unsaturated conductivity with depth was essentially controlled by the proportion of air-filled pores. More recently, Turberg et al. (2014) used X-ray μ-CT to analyze various degrees of disturbance related to the process of peat extraction, working with large samples $15\times15\times45$ cm^3 in volume and a medical X-ray scanner. 3-D images of regular parallelepipeds $2\times2\times14$ cm^3 in volume were recorded with a resolution of 371 μm.

Because of the low consistency of peat materials, and consequently of the possible alteration of the structure during sub-sampling in the peat blocks collected in the field, several authors used freezing before extraction to avoid deformation during sub-sampling. This strategy gives small undisturbed samples, making it possible to increase the resolution of the 3D X-ray μ-CT images recorded. The peat samples collected by Kettridge and Binley (2008) were frozen soon after collection, and then defrosted prior to their study but the reason for freezing the samples remains unclear, and appears to have been motivated more by storage conditions than by the sub-sampling methodology. Quinton et al. (2009) and Rezanezhad et al. (2010) froze peat blocks at –10°C for 48h before sub-sampling cores 10 cm long and 6 cm in diameter which were extracted using a hollow drill bit mounted on a drill press. Gharedaghloo et al. (2018) used data from Rezanezhad et al. (2009 and 2010) and modeled water and solute transport in the pore network of $9.92\times9.92\times9.92$ mm^3 samples extracted from X-ray μ-CT images of the peat materials. They showed that the decrease in the hydraulic conductivity with depth was related to the reduction in

pore radius and increase in tortuosity. Improvements in the X-ray μ-CT technique have led to an increase in the image resolution, requiring the use of smaller-sized samples; this evolution will inevitably lead to an increasing recourse to a freezing phase to obtain samples with the appropriate size before analysis.

The question arises, however, whether freezing impacts the evolution of the soil structure. When water passes from the liquid to the solid state, its volume increases by 8.7% (the density of ice is 0.92 g mL^{-1} while that of the liquid is 1 g mL^{-1}). Investigating on the effects of freezing on the physical properties and wettability of highly decomposed peats used as growing media, Michel (2015) showed that freezing was accompanied by a decrease in bulk density and a marked change in the water retention properties but the pore structure was not analyzed. Wang et al. (2017) used X-ray μ-CT and showed that non-uniform volumetric shrinkage, referred to as the freeze-necking phenomenon, was observed in an unsaturated clay soil in a closed freeze-thaw experiment. Liu et al. (2021) studied the impact of freeze-thaw cycles on the pore structure characteristics of silty soil using X-ray μ-CT with a 25 μm resolution on the volume of interest, namely 8.75×8.75×8.75 mm^3. Results showed an increase in the macroporosity and pore-throat network complexity. Ma et al. (2021) studied the effect of freeze-thaw cycles on the pore distribution in soil aggregates 5-7 mm in diameter using the 3D images with 3.25 μm resolution produced by synchrotron-based X-ray μ-CT. Results showed how the creation of pores resulting from freeze-thaw cycles can explain changes in the stability of aggregates.

As the properties of porous materials are controlled by macro- and micro-pore distribution and topology (Vogel, 2002), it is important to pay close attention to the quality of the pore distribution and topology description resulting from X-ray μ-CT analysis. The latter can only be used to study the air-filled pores, as those occupied by water are being very difficult to distinguish from the water-saturated organic matrix. The possible alteration of both the pore network geometry and its saturation degree during sample preparation therefore remains a concern. However, little attention has been paid to the possible alteration of the pore network during sample preparation which requires freezing to obtain subsamples with a size suitable for the desired resolution with the X-ray μ-CT used. As freezing is nowadays increasingly used to obtain small size samples of peat materials for X-ray μ-CT analysis, the objective of this study was to analyze a highly decomposed peat material before freezing and post-defreezing using X-ray μ-CT to assess whether freezing modified its structure or not by analyzing the air-filled pores before and after the freeze-thaw process.

2 Materials and methods

2.1 Field sampling

Highly decomposed *Sphagnum* and *Molinia* peat was sampled in duplicate (samples A and B) in sites which were intensively studied by D'Angelo et al. (2016), Bernard-Jannin et al. (2018) and Leroy et al. (2018, 2019a and 2019b). A highly decomposed peat was selected for study because it is potentially highly sensitive to the creation of structure artifacts during freezing due to its high water content and low fiber content. Large undisturbed samples (15×15×25 cm^3) were collected between 25 and 40 cm depth to avoid the heterogeneity of the top 20 cm due to *Molinia* roots. They were collected when the groundwater table level was close to the soil surface. The samples were stored at 3–4 °C to limit biological activity and in sealed plastic bags to avoid water loss.

2.2 Physico-chemical analysis

Bulk density and particle density were determined by using undisturbed peat samples a dozen cubic centimeters in volume and the kerozene method developed by Monnier et al. (1973). The total porosity was obtained by dividing the volume of water contained in a saturated sample by the known volume of the sample as described by Boelter (1976) and Nimmo (2013). The water content of the collected samples was determined after oven drying at 105°C for 24h. The degree of peat decomposition was characterized with the pyrophosphate index (Kaila 1956) which was determined following Gobat et al. (1986). The C and N contents were determined by combustion of dried and crushed samples at 1100°C, using a CNS-2000 LECO apparatus.

2.3 Sub-sampling in the laboratory

In order to have samples of the appropriate size for X-ray µ-CT, sub-samples of peat materials 4×4×7 cm^3 in volume corresponding to the depth of 30–37 cm were prepared by cutting with a scalpel blade to limit disturbance of the peat structure as far as possible. Then, each sample was placed in a transparent PVC tube 5 cm in diameter which was then hermetically sealed with a screw cap to avoid water loss. They were first imaged by X-ray µ-CT and then, on the basis of the methodology developed and used by Rezanezhad et al. (2010), Ramirez et al. (2016) and Moore et al. (2017), they were frozen at -10°C for 48 h, defrosted for 48 h at 20°C and imaged again by X-ray µ-CT. Each sealed PVC tube with its peat material was weighed at the different steps of the process, i.e. prior and after each X-Ray µ-CT imaging, to check the absence of water loss during the acquisition of the projected 2D images. Measurements showed that the weight variation between two successive steps and between the first and last step was <0.03 g for the two samples studied. This amount loss was considered negligible.

2.4 X-ray Computed Tomography imaging (2D and 3D images)

X-ray µ-CT was performed for the sub-samples 4×4×7 cm^3 in volume using a micro X-ray µ-CT device Nanotom 180NF (GE Phoenix|x-ray, Wunstorf, Germany). This equipment has a 180-kV nanofocus X-ray tube and a digital detector array (2304×1152 pixels, Hamamatsu detector). Samples were placed in the chamber and rotated by 360 degrees during acquisition. The samples were centered and waxed on a sample holder (circular plate) whose axis of rotation was collinear to that of the tomograph chuck. An operating voltage of 120 kV and a filament current of 100 µA were applied. The distance between the X-ray source and the sample and between the X-ray source and the detector was 300 and 500 mm, respectively, giving a voxel size of 60 µm. The tomograph detector recorded 2D projections in 16 bit, i.e. divided into 65536 grey levels. The resulting projections were converted into a 3D image stack using a microcluster of four personal computers (PCs) with the Phoenix 3D reconstruction software. A filtered backprojection algorithm was used according to Feldkamp et al. (1984). The reconstruction software contained several different modules for artifact reduction (beam hardening, ring artifacts) to optimize the results. After reconstruction, the images were recorded in 8 bit (256 levels of grey) by always checking that the histograms of the 16-bit and 8-bit images were similar and that the images visually indistinguishable. During this process, we increased the dynamic range of the image by spreading the histogram over the entire range between 0 and 255 levels of grey. This facilitated the subsequent segmentation step. The 2000 projection images (angular increment

144 of 0.18°) were acquired during sample rotation (with an acquisition time of 4 hours) for every sample before
145 freezing and post-defreezing. As the cone beam geometry created artifacts, the first and the last 76 cross-sectional
146 images were removed (Le Trong et al., 2008; Rozenbaum and Rolland du Roscoat, 2014).
147 The resulting 3D images were cropped for sample A to a size of 430×600×800 voxels corresponding to
148 2.6×3.6×4.8 cm^3 before freezing and post-defreezing, and for sample B to a size of 430×530×850 voxels before
149 freezing and post-defreezing corresponding to 2.6×3.2×5.1 cm^3, each image in a local 3D coordinate system with
150 a voxel size of 60×60×60 μm^3 for samples A and B before freezing and post-defreezing.

151 **2.5 X-ray image analysis (segmentation and attenuation)**

152 A region of interest that excluded the irregular sample boundaries and outside region was defined for every sample
153 by identifying the largest rectangular parallelepiped image in the cylindrical sample studied. Smoothing the 3D
154 images with a moving average filter over a window of 5×5×5 voxels increased their signal-to-noise ratios from the
155 range [7.6-9.2] to [12.5-15.0]. The moving average filter replaced each voxel of the original image by the average
156 grey value of its neighbors over a window centered on it as this is considered the optimal method to remove random
157 noise on grey-level images (Smith, 1997). The signal-to-noise ratio was computed as being the ratio of the average
158 of the grey levels of the image to their standard deviation according to Avcibas et al. (2002). They were then
159 segmented by thresholding. The threshold value used was the absolute minimum between the two peaks of the
160 bimodal distribution of the grey levels of the voxels of each image (Fig. 1) (Rozenbaum et al., 2012). The grey
161 level corresponding to the threshold value for sample A before freezing and post-defreezing was 93 and 78
162 (Fig. 1a), respectively, and for sample B before freezing and post-defreezing, it was 80 and 68, respectively (Fig.
163 1b). The voxels with a grey level smaller than the threshold value were considered as being pore voxels while
164 those with a grey level higher than or equal to the threshold value were considered as matrix voxels. This simple
165 procedure has no adjustable parameter and therefore introduces no bias when comparing the images. In each binary
166 image, each pore (i.e. group of contiguous foreground voxels surrounded by matrix voxels) was identified by a
167 voxel-by-voxel scanning of the image, and its volume (in terms of number of voxels) recorded by the following
168 algorithmic procedure:

169 - Consider each voxel during a raster scan of the image. Let *v* be the current voxel;
170 - If *v* is a matrix voxel, or has been marked as belonging to an already identified pore, proceed to the next
171 voxel;
172 - If *v* is a pore voxel belonging to a yet unidentified pore, starting from *v*, perform a geodesic reconstruction
173 of the pore (Lantuéjoul and Beucher, 1981). During the reconstruction of the pore, mark all its voxels as

belonging to an identified pore, and keep count of their number. Once the reconstruction is complete, the number of voxels yields the volume of the pore. Proceed to the next voxel in the raster scan.

The outcome of this procedure is list of pores, of their volume and their position in the 3D image. The total porosity is then the ratio of the total pore volume divided by the total volume of the rectangular parallelepiped selected.

3 Results and discussion

3.1 Characteristics of the peat samples studied

The measured physical characteristics of the peat samples studied are given in Table 1. The volumetric water contents at sampling were similar for the two samples A and B (0.893 and 0.883 cm^3 cm^{-3}, respectively). These values are much higher than those recorded by Rezanezhad et al. (2010) for sphagnum peat materials (between 0.38 and 0.43 cm^3 cm^{-3}) collected between the surface and 67 cm depth. Their peat materials were collected far from water saturation because the groundwater table level was far from the surface, whereas our samples were collected with a groundwater table level close to the soil surface. The porosity values of samples A and B (0.918 and 0.904, respectively) are close to their water content, thus indicating that they are close to water saturation. The measured bulk densities recorded for the two samples A and B (0.135 to 0.178 g cm^{-3}, respectively) are consistent with those of highly decomposed peat materials (Benscoter et al., 2011; Kurnain and Hayati, 2016). The measured pyrophosphate indices recorded for samples A and B (96.1 and 78.9, respectively) are also consistent with highly decomposed peat materials which can be classified as asapric peat (pyrophosphate index >30) according to Levesque et al. (1980). The C/N ratio recorded for samples A and B (12.1 and 16.6, respectively) confirms that the two peat samples present a high degree of decomposition (Comont et al. 2006). Finally, the dry bulk density values recorded for the two samples A and B (0.135 and 0.178 g cm^{-3}, respectively) are much closer to the values recorded for a well-decomposed peat material resulting from *Sphagnum* moss with a fiber content of only 15% (0.250 g cm^{-3}) than to the values recorded for undecomposed peat materials with a fiber content of 98% (0.009 g cm^{-3}) (Boelter, 1968). Overall, the peat material selected for this study is much more decomposed than the peat materials studied by Quinton et al. (2009) and Rezanezhad et al. (2010).

3.2 Comparison of the 2D and 3D X-ray μ-CT images in grey levels before freezing and post-defreezing

The same heights were chosen for the 3D X-ray μ-CT images in grey levels before freezing and post-defreezing for samples A (800 voxels) and B (850 voxels). The final image sizes chosen were then 430×600×800 voxels (~2.6×3.6×4.8 cm^3) before freezing and post-defreezing for sample A and 430×530×850 voxels (~2.6×3.2×5.1 cm^3) before freezing and post-defreezing for sample B.

The grey level on the images was determined by the absorption of the incident X-ray radiation by the different phases of the peat material. The absorption of each phase depends on its density and mean atomic number resulting from its chemical composition (Youn et al., 2015). It is described by the Beer-Lambert Law:

$$I = I_o \, exp(-\mu x) \quad (1)$$

where I is the transmitted X light, I_o the incident X light, μ the absorption coefficient, and x the path length. Consequently, the intensity of the transmitted X light which results in a grey level of the pixel in the 2D images and of the voxel in the 3D images depends on the proportion of air, water and organic compounds in the pixel or voxel considered. Because of the weak difference between the mean atomic number assumed for the porous organic matrix of a highly decomposed and water-saturated peat material (Table 1) and the mean atomic number of the water phase, we can assume that the absorption coefficient of these two phases is very close. Therefore, only the air phase can be distinguished from the other phases. Thus, only the air-filled pores are identifiable on the 2D and 3D images; the pores occupied by water are undistinguishable from the water-saturated porous organic matrix. Pairs of 2D X-ray µ-CT images recorded before freezing and post-defreezing were selected within the pairs of stacks of 2D images by identifying the closest images in terms of morphology of air-filled pores a few hundred micrometers in size. These pores are shown in very dark grey in Fig. 2. The lighter dark grey background corresponds to the highly decomposed organic material and related porosity which was filled by water. For each pair of 2D X-ray µ-CT images, comparison showed the presence of (i) pores recognizable on the images before freezing which were still present post-defreezing but exhibiting a different morphology, (ii) pores recognizable on the images before freezing which were not present post-defreezing, (iii) and the presence of pores recognizable post-defreezing and which were not present before freezing (Fig. 2). However, the use of pairs of 2D X-ray µ-CT images does not enable an accurate estimation of the possible evolution of the porosity of peat materials during the freezing process since it was not possible to say whether the pairs of 2D images corresponded exactly to the same slice in the sample before and post-defreezing. Only a 3D analysis is able to establish whether the porosity of the peat materials is different before and post-defreezing.

3.3 Comparison of 3D CT binary images before freezing and post-defreezing

The 3D X-ray µ-CT binary images of the two samples A and B were first morphologically compared globally by comparing the porosity characterized in X-ray µ-CT before freezing and post-defreezing (Figs. 3a and d, 4a and d). Results showed that the air-filled pores measured corresponded to a very small proportion of the total porosity of the peat material studied, less than 0.02, whereas the total porosity of samples A and B determined by using the water content when the samples were saturated was 0.918 and 0.904 before freezing, respectively (Tables 1 and 2). Most of the porosity corresponded to both water-filled pores associated to the highly decomposed organic compounds and potentially to larger water-filled pores that were indistinguishable from the porous organic matrix. The number of air-filled pores was however very different before freezing and post-defreezing for the two samples studied. There were 470 and 474 air-filled pores before freezing, and 4792 and 4371 air-filled pores post-defreezing for samples A and B, respectively (Table 2). Whatever the origin of the new air-filled pores, results showed a strong decrease in the average size of the air-filled pores post-defreezing, from 3952 to 732 voxels and from 2043 to 488 voxels for samples A and B, respectively (Table 2).

Analysis of the pore size distribution showed that the increase in the number of air-filled pores was mainly related to an increase in the number of pores <500 voxels in volume (i.e. <0.108 mm^3) (Figs. 5a, b, c and d). Air-filled pores >500 voxels were also highly affected (Figs. 5a', b', c' and d'). After separation of the air-filled pores larger and smaller than 500 voxels in volume, the 3D X-ray µ-CT images showed that the morphology of the air-filled pores >500 voxels was affected, with alterations in both their continuity and transversal section size (Figs. 3c and

f, 4c and f). Analysis of the distribution of the pores <500 voxels in volume showed a strong increase in the number of pores in all sizes, with the highest increase recorded for pores ranging from 1 to 50 voxels in volume (Fig. 6). Sub-images of the 3D X-ray µ-CT images recorded were selected to compare the difference in pore morphology qualitatively before freezing and post-defreezing more easily than with the whole images in which the high number of pores limited the morphological analysis (Figs. 3 and 4), particularly for the pores <500 voxels (Figs. 3b and e, 4b and e). Thus, one 3D X-ray µ-CT sub-image 200×350×350 voxels in volume (~1.2×2.1×2.1 cm^3) and another one 300×300×300 voxels in volume (~1.8×1.8×1.8 cm^3) were selected for samples A and B, respectively (Figs. 7 and 8). The selected sub-images showed that the pores <500 voxels corresponded to air-filled pores of several voxels to several dozen voxels, and to discontinuous air-filled fine tubular pores (Figs. 7b and e, 8b and e). The comparison showed that freezing led to a dramatic increase in the number of air-filled pores (Figs. 7 and 8) and to the appearance or disappearance of discontinuous air-filled fine tubular pores <500 voxels (Figs. 7b and e, 8b and e).

3.4 Origin of the difference recorded before freezing and post-defreezing

As freezing leads to an 8.7% increase in the specific volume of the water, the possible consequences of this increase on the changes recorded for the peat material studied were analyzed. The total porosity before freezing ($\phi_{T,\,BF}$) can be written as follows:

$$\phi_{T,BF} = V_{V,\,BF} / (V_S + V_{V,BF}) \quad (2)$$

where $V_{V,\,BF}$ is the total specific volume of pores of the peat material before freezing in $cm^3\ g^{-1}$, V_S is the specific volume of the organic solid phase dried at 105°C in $cm^3\ g^{-1}$ and equal to 0.591 $cm^3\ g^{-1}$ and 0.562 $cm^3\ g^{-1}$ for samples A and B, respectively (reciprocal of the particle density measured for peat materials A and B) (Table 1). Thus, using equation (2):

$$V_{V,\,BF} = \phi_{T,\,BF} \times V_S / (1 - \phi_{T,\,BF}) \quad (3)$$

which gives $V_{V,\,BF}$ = 6.616 $cm^3\ g^{-1}$ and 5.292 $cm^3\ g^{-1}$ for samples A and B, respectively. The specific volume of pores before freezing, $V_{V,\,BF}$, can be decomposed as follows:

$$V_{V,\,BF} = V_{V,\,Mwf,\,BF} + V_{V,\,TPwf,\,BF} + V_{V,\,TPaf,\,BF} \quad (4)$$

where $V_{V,\,Mwf,\,BF}$ is the specific volume of pores of the organic matrix saturated with water before freezing in $cm^3\ g^{-1}$, $V_{V,\,TPwf,\,BF}$ is the specific volume of tubular pores occupied with water before freezing in $cm^3\ g^{-1}$ and $V_{V,\,TPaf,\,BF}$ is the specific volume of tubular air-filled pores before freezing in $cm^3\ g^{-1}$. The porosity related to the tubular air-filled pores before freezing, $\phi_{TPaf,\,BF}$, in the whole peat material is:

$$\phi_{TPaf,\,BF} = V_{V,\,TPaf,\,BF} / (V_S + V_{V,\,BF}) \quad (5)$$

Thus:

$$V_{V,\,TPaf,\,BF} = \phi_{TPaf,\,BF} \times (V_S + V_{V,\,BF}) \quad (6)$$

which gives $V_{V,\,TPaf,\,BF}$ = 0.065 $cm^3\ g^{-1}$ and 0.029 $cm^3\ g^{-1}$ for samples A and B, respectively, with the values of $\phi_{TPaf,\,BF}$ corresponding to the value of ϕ measured before freezing using X-ray µ-CT (Table 2).

The increase in the specific volume of liquid water by 8.7% when it turns to solid from 20°C to –10°C (Harvey, 2017) increases the porosity of both the pores in the organic matrix and the tubular pores fillled with water before freezing to a porosity post-defreezing which can be calculated as follows:

$$\phi_{Mwf,\,AF} + \phi_{TPwf,\,AF} = [(V_{V,\,Mwf,\,BF} + V_{V,\,TPwf,\,BF}) \times 1.087] / [V_S + ((V_{V,\,Mwf,\,BF} + V_{V,\,TPwf,\,BF}) \times 1.087) + V_{V,\,TPaf,\,BF}] \quad (7)$$

where $\phi_{Mwf,\,AF}$ is the porosity related to the water-filled of the organic matrix post-defreezing, $\phi_{TPwf,\,AF}$ is the porosity related to the water-filled tubular pores post-defreezing, and 1.087 the coefficient by which the volume of water is increased when it turns from liquid (20°C) to solid (–10°C). Using equation (4):

$$\phi_{Mwf,\,AF} + \phi_{TPwf,\,AF} = [(V_{V,\,BF} - V_{V,\,TPaf,\,BF}) \times 1.087] / [V_S + ((V_{V,\,BF} - V_{V,\,TPaf,\,BF}) \times 1.087) + V_{V,\,TPaf,\,BF}] \quad (8)$$

which gives $\phi_{Mwf,\,AF} + \phi_{TPwf,\,AF} = 0.916$ and 0.906 for peat materials A and B, respectively by using values of $V_{V,\,BF}$ and $V_{V,\,TPaf,\,BF}$ given by equations (3) and (6), respectively. These values can be compared to those of $\phi_{Mwf,\,BF} + \phi_{TPwf,\,BF}$ before freezing that were calculated as follows:

$$\phi_{Mwf,\,BF} + \phi_{TPwf,\,BF} = \phi_T - \phi_{TPaf,\,BF} \quad (9)$$

with $\phi_{TPaf,\,BF}$ equal to ϕ before freezing (Table 2), which gives $\phi_{Mwf,\,BF} + \phi_{TPwf,\,BF} = 0.909$ and 0.899 for samples A and B, respectively. Thus, according to these results and the related assumptions, the increase in the water-filled porosity of samples A and B post-defreezing was 0.007. These values can be compared with the increase in the air-filled porosity and measured with the 3D X-ray μ-CT images recorded in this study. This increase post-defreezing was 0.008 and 0.006 for samples A and B, respectively and thus similar to the calculated values.

Based on these different results, two scenarios can be proposed to explain what happened during the freeze-thaw process. According to the first scenario, during freezing, the water-filled pore volume corresponding to the sum of the pores of the organic matrix and of fine tubular pores increases by 8.7% because of the increase in the specific volume of water when it turns from liquid to solid. After thawing to room temperature, the peat material keeps the memory of this evolution during the freezing phase. As the specific pore volume of the highly decomposed organic matrix increases in volume following the formation of ice, it does not then decrease after thawing, with the result that the water, which is located preferentially in the smallest pores, small tubular pores and largest pores of the organic matrix, all saturated with water before freezing, is no longer located in these pores when the water turns from solid to liquid after thawing. The porosity newly occupied by air was measured by using 3D X-ray μ-CT (Table 2) and corresponds to the increase in porosity calculated following the transformation of liquid water into ice. The second scenario assumes that most of the small elongated pores would be already partially air-filled but their volumes are too small to be detected with the 3D X-ray μ-CT used in this study. After the freeze-thaw process for the same reasons as for the first scenario concerning the evolution of the porous organic matrix, the proportion and size of small air-filled pores increases, making them detectable by 3D X-ray μ-CT.

Finally, the increase in the specific volume of water because of freezing may also be responsible for the alteration of the already air-filled tubular pores >500 voxels before freezing as shown by the 3D binary images (Figs. 3 and 4) and the pore volume distribution (Figs. 5 and 6) because of deformations in the structure of the surrounding porous organic matrix during freezing.

4. Conclusions

Our results show that the freezing technique that can be used prior to peat material sub-sampling as required by 3D X-ray μ-CT altered the structure of the highly decomposed and close to water saturation peat material studied. Both the continuity and cross section of the tubular pores measuring from several hundreds to about one thousand micrometers in diameter differed before freezing and post-defreezing. These pores were several hundreds to several thousand voxels in volume in the 40 cm^3 highly decomposed peat material studied, one voxel corresponding to 216 μm^3 in volume. Results also show that very small air-filled pores several voxels to several dozen voxels in volume and discontinuous air-filled fine tubular pores within the peat material studied were only detected post-defreezing in the samples. The increase in the specific volume of water by 8.7% when it turns from liquid to solid because of freezing led to the creation of a pore volume in the organic matrix which remained saturated by water when returning to room temperature. This induced the desaturation of some of the finest tubular pores as well as some the largest pores of the porous organic matrix which were both water-filled before freezing. The volume of these pores newly occupied by air post-defreezing was measured using X-ray μ-CT and their cumulated volume was found to be consistent with the one calculated by taking into account the thermal expansion of water from 20°C (liquid) to –10°C (ice). We conclude that the increase in the specific volume of water because of freezing is also responsible for the alteration of the already air-filled tubular pores >500 voxels before freezing, as shown by the 3D binary images and the pore volume distribution, and that this alteration is a consequence of the deformation of the organic matrix due to the increase in the specific volume of water when it turns from liquid to solid because of freezing. Finally, our results show clearly that both the pore morphology and pore size distribution, and more globally the structure of the highly decomposed peat material studied, were altered by freezing. Thus, the possible consequences of freezing prior to any study of the structure of peat materials should be investigated, particularly for highly decomposed peat materials. Future work will focus on the possible presence of pore geometry artifacts similar to those recorded in our study in less decomposed peat materials, which may be less sensitive to the occurrence of artefacts post-defreezing.

Financial support. This research was supported by the Labex Voltaire (ANR-10-LABEX-100-01) and the French program PAUSE.

Acknowledgements. The authors acknowledge Dr. Sébastien Gogo for his assistance during field sampling, Marielle Hatton for her contribution to chemical analysis and Philippe Penhoud for his contribution to X-ray μ-CT image acquisition.

References

Avcibas, I., Sankur, B., and Sayood, K.: Statistical evaluation of image quality measures, J. Electron. Imag., 11(2), https://doi.org/10.1117/1.1455011, 2002.

Benscoter, B. W., Thompson, D. K., Waddington, J. M., Flannigan, M. D., Wotton, B. M., de Groot, W. J., and Turetsky, M. R.: Interactive effects of vegetation, soil moisture and bulk density on depth of burning of thick organic soils, Int J Wildland Fire., 20, 418–429, https://doi.org/10.1071/WF08183, 2011.

Bernard-Jannin, L., Binet, S., Gogo, S., Leroy, F., Défarge, C., Jozja, N., Zocatelli, R., Perdereau, L., and Laggoun-Défarge, F.: Hydrological control of dissolved organic carbon dynamics in a rehabilitated Sphagnum dominated peatland: a water-table based modelling approach, Hydrol Earth Syst Sc., 22, 4907–4920, https://doi.org/10.5194/hess-2017-578 , 2018.

Boelter, D. H.: Important physical properties of peat materials, Proceedings of the 3rd Int Peat Cong, Quebec, 150–154, 1968.

Boelter, D. H.: Methods for analysing the hydrological characteristics of organic soils in marsh-ridden areas. In: Hydrology of Marsh-Ridden Areas, Proceedings of IASH Symposium Minsk, 1972, IASH, UNESCO, Paris, 161–169, 1976.

Comont, L., Laggoun-Défarge, F., and Disnar, J. R.: Evolution of organic matter indicators in response to major environmental changes: the case of a formerly cut-over peat bog (Le Russey, Jura Mountains, France), Org Geochem. 37, 1736–1751. https://doi.org/10.1016/j.orggeochem.2006.08.005, 2006

D'Angelo, B., Gogo, S., Laggoun-Défarge, F., Le Moing, F., Jégou, F., and Guimbaud, C.: Soil Temperature Synchronisation improves representation of diel variability of Ecosystem Respiration in Sphagnum Peatlands, Agr Forest Meteorol., 223, 95–102, https://doi.org/10.1016/j.agrformet.2016.03.021, 2016.

Feldkamp, L.A., Davis, L.C., and Kress, J.W.: Practical cone-beam algorithm, J. Opt. Soc. Am. A, 1(6), https://doi.org/10.1364/JOSAA.1.000612, 1984.

Gharedaghloo, B., Price, J. S., Rezanezhad, F., and Quinton, W. L.: Evaluating the hydraulic and transport properties of peat soil using pore network modeling and X-ray micro computed tomography, J. Hydrol., 561, 494–508, https://doi.org/10.1016/j.jhydrol.2018.04.007, 2018.

Glaser, P.H., Rhoades, J., and Reeve, A.S.: The hydraulic conductivity of peat with respect to scaling, botanical composition, and greenhouse gas transport: mini-aquifer tests from the Red Lake Peatland, Minnesota, J. Hydrol., 596, 125686, https://doi.org/10.1016/j.hydrol.2020.125686, 2021.

Gobat, J. M., Grosvernier, P., and Matthey, Y.: Les tourbières du Jura suisse. Milieux naturels, modifications humaines, caractères des tourbes, potentiel de régénération, Actes de la Société Jurassienne d'Emulation, 213–315, 1986.

Harvey, A. H.: Properties of ice and supercooled water. In: Haynes W M, Lide D R., Bruno T J. (eds.). CRC Handbook of Chemistry and Physics (97th ed.), Boca Raton, FL, CRC Press, 2017.

Helliwell, J. R., Sturrock, C. J., Grayling, K. M., Tracy, S. R., Flavel, R. J., and Young, I. M.: Applications of X-ray computed tomography for examining biophysical interactions and structural development in soil systems: a review, Eur. J. Soil Sci. 64, 279–297, https://doi.org/10.1111/ejss.12028, 2013.

Kaila, A.: Determination of the degree of humification of peat samples, J. Agr. Sci. Finland, 28, 18–35, 1956.

Kettridge, N., and Binley, A.: X-ray computed tomography of peat soils: measuring gas content and peat structure, Hydrol. Process., 22, 4827–4837, https://doi.org/10.1002/hyp.7097, 2008.

Kettridge, N., and Binley, A.: Characterization of peat structure using X-ray computed tomography and its control on the ebullition of biogenic gas bubbles, J. Geophys. Res., 116, G01024, https://doi.org/10.1029/2010JG001478, 2011.

Kurnain, A., and Hayati, A.: Characteristics of water retention of ombrotrophic peats under different land uses, Full Paper Proceedings ETAR, Int. Conf. on Emerging Trends in Academic Research, 3, 271–280, http://eprints.ulm.ac.id/id/eprint/3165, 2016.

Lantuéjoul, C., and Beucher, S.: On the use of the geodesic metric in image analysis. J. Microsc., 121, 39-49, 1981.

Leroy, F., Gogo, S., Buttler, A., Bragazza, L., and Laggoun-Défarge, F.: Litter decomposition in peatlands is promoted by mixed plants, J. Soils Sediments, 18, 739–749, https://doi.org/10.1016/j.jes.2018.08.003, 2018.

Leroy, F., Gogo, S., Guimbaud, C., Francez, A. J., Zocatelli, R., Défarge, C., Bernard-Jannin, L., Hu, Z., and Laggoun-Défarge, F.: Response of C and N cycles to N fertilization in Sphagnum and Molinia-dominated peat mesocosms, J. Environ. Sci., 77, 264–272, https://doi.org/10.1016/j.jes.2018.08.003, 2019a.

Leroy, F., Gogo, S., Guimbaud, C., Bernard-Jannin, L., Yin, X., Belot, G., Shuguang, W., and Laggoun-Défarge, F.: CO_2 and CH_4 budgets and global warming potential modifications in *Sphagnum*-dominated peat mesocosms invaded by *Molinia caerula*, Biogeosciences, 16, 4085-4095. https://doi.org/10.5194/bg-16-4085-2019, 2019b.

Le Trong, E., Rozenbaum, O., Rouet, J. L., and Bruand, A.: A simple methodology to segment X–ray tomographic images of a multiphasic building stone, Image Anal. Stereol., 27, 175–182, https://doi.org/10.5566/ias.v27.p175-182, 2008.

Levesque, M., Dinel, H., and Marcoux, R.: Évaluation des critères de différentiation pour la classification de 92 matériaux tourbeux du Québec et de l'Ontario, Can. J. of Soil Sci., 60, 479–486. https://doi.org/10.4141/cjss80-053, 1980.

Liu, B., Ma, R. M., and Fan, H. M.: Evaluation of the impact of freeze-thaw cycles on pore structure characteristics of black soil using X-ray computed tomography, Soil Till. Res., 206, 104810, https://doi.org/10.1016/j.still.2020.104810, 2021.

Ma, R. M., Jiang, Y., Liu, B., and Fan, H. M. Effects of pore structure characterized by synchrotron-based micro-computed tomography on aggregate stability of black soil under freeze-thaw cycles, Soil Till. Res., 207, 104855, https://doi.org/10.1016/j.still.2020.104855, 2021.

Michel, J. C., Rivière, L. M., and Bellon-Fontaine, M. N. : Measurement of the wettability of organic materials in relation to water content by capillary rise method, Eur. J. Soil Sci., 52, 459–467, https://doi.org/10.1046/j.1365-2389.2001.00392.x, 2001.

Michel, J. C.: Effect of freezing on the physical properties and wettability of highly decomposed peats used as growing media, Eur. J. Hortic. Sci., 80, 190–195, doi: 10.17660/eJHS.2015/80.4.7, 2015.

Monnier, G., Stengel, P., and Fiès, J. C. : Une méthode de mesure de la densité apparente de petits agglomérats terreux. Application à l'analyse des systèmes de porosité du sol, Ann. Agron., 25, 533–545, 1973.

Moore, P. A., Lukenbach, M. C., Kettridge, N., Petrone, R. M., Devito, K. J., and Waddington, J. M.: Peatland water repellency: Importance of soil water content, moss species, and burn severity, J. Hydrol., 554, 656–665, https://doi.org/10.1016/j.jhydrol.2017.09.036, 2017.

Müller, J., and Fortunat, J.: Committed and projected future changes in global peatlands – continued transient model simulations since the Last Glacial Maximum, Biogeosciences, 3657–3687, https://doi.org/10.5194/bg-18-3657-2021, 2021.

Nimmo, J. R.: Porosity and pore size distribution, Enc. Soil Environ., 3, 295–303, https://doi.org/10.1016/B978-0-12-409548-9.05265-9, 2013.

Quinton, W. L., Elliot, T., Price, J. S., Rezanezhad, F., and Heck, R.: Measuring physical and hydraulic properties of peat from X-ray tomography, Geoderma, 153, 269–277, https://doi.org/10.1016/j.geoderma.2009.08.010, 2009.

Ramirez, J. A., Baird, A. J., and Coulthard, T. J.: The effect of pore structure on ebullition from peat, J. Geophys. Res-Biogeo., 121, 1646–1656. https://doi.org/10.1002/2015LG003289, 2016.

Rezanezhad, F., Quinton, W. L., Price, J. S., Elrick, D., Elliot, T. R., Heck, R. J.: Examining the effect of pore size distribution and shape on flow through unsaturated peat using 3-D computed tomography, Hydrol. Earth Syst. Sci., 13, 1993–2002, https://doi.org/10.5194/hess-&"-1993-2009, 2009.

Rezanezhad, F.., Quinton, W. L., Price, J. S., Elliot, T. R., Elrick, D., and Shook, K. R:. Influence of pore size and geometry on peat unsaturated hydraulic conductivity computed from 3D computed tomography image analysis, Hydrol. Process., 24, 2983–2994, https://doi.org/10.5194/hess-13-1993-2009, 2010.

Rozenbaum, O., Bruand, A., and Le Trong, E. : Soil porosity resulting from the assemblage of silt grains with a clay phase: New perspectives related to utilization of X-ray synchrotron computed microtomography, C.R. Geosci., 344, 516–525, https://doi.org/10.1016/j.crte.2012.09.004, 2012.

Rozenbaum, O., and Rolland du Roscoat, S.: Representative elementary volume assessment of three-dimensional x-ray microtomography images of heterogeneous materials: Application to limestones, Phys. Rev. E 89: 053304. https://doi.org/10.1103/PhysRevE.89.053304, 2014.

Smith, S. W.: The scientist and engineer's guide to digital signal processing. California Technical Publishing, USA, 1997.

Swinnen, W., Broothaerts, N., and Verstraeten G.: Modelling long-term alluvial peatland dynamic in temperate river flood plains, Biogeosciences Discuss [preprint], https://doi.org/10.5194/bg-2021-132, in review, 2021.

Turberg, P., Zeimetz, F., Grondin, Y., Elandoy, C., and Buttler, A.: Characterization of structural disturbances in peats by X-ray CT-based density determinations, Eur. J. Soil Sci., 65, 613–624. https://www.dora.lib4ri.ch/wsl/islandora/ object/wsl:5128, 2014.

Vogel, H. J.: Topological characterization of porous media. 2nd International Wuppertal Workshop on Statistical Physics and Spatial Statistics, university of Wuppertal, Wuppertal, Germany, March 05–09, 2001, In Mecke K and Stoyan D (eds) Morphology of condensed matter: Physics and geometry of spatially complex systems, Lecture Notes in Physics, Springer, 600, 75 – 92, 2002.

Wang, S., Yang, Z., and Yang, P.: Structural change and volumetric shrinkage of clay due to freeze-thaw by 3D X-ray computed tomography, Cold Reg. Sci. Technol., 138, 108–116. https://doi.org/10.1016/j.coldregions.2017.03.007, 2017.

Wiedeveld, S.Th.J., van den Berg, M., and Lamers, L.P.M.: Conventional subsoil irrigation techniques do not lower carbon emissions from drained peat meadows, Biogeosciences, 18, 3881–3902, https://doi.org/10.5194/bg-18-3881-2021, 2021.

Youn, H., Kim, H. K., Kam, S., Kim, S. H., Park, J. W., and Jeon, H.: Physics-based modeling of computed tomography systems, Conference on Medical Imaging – Physics of Medical Imaging, Orlando, FL, Feb 22–25, 2015, In: Hoeschen C and Kontos D (eds) Medical imaging 2015: Physics of medical imaging. Proceedings of SPIE, 9412: 94122N, 2015.

Zhao, H.F., Muraro, S., and Jommi C.: Gas exsolution and gas invasion in peat: towards a comprehensive modelling framework, Géotechnique Letters, 10(3), 461-467, https://doi.org/10.1690/jgele.20.00014, 2020.

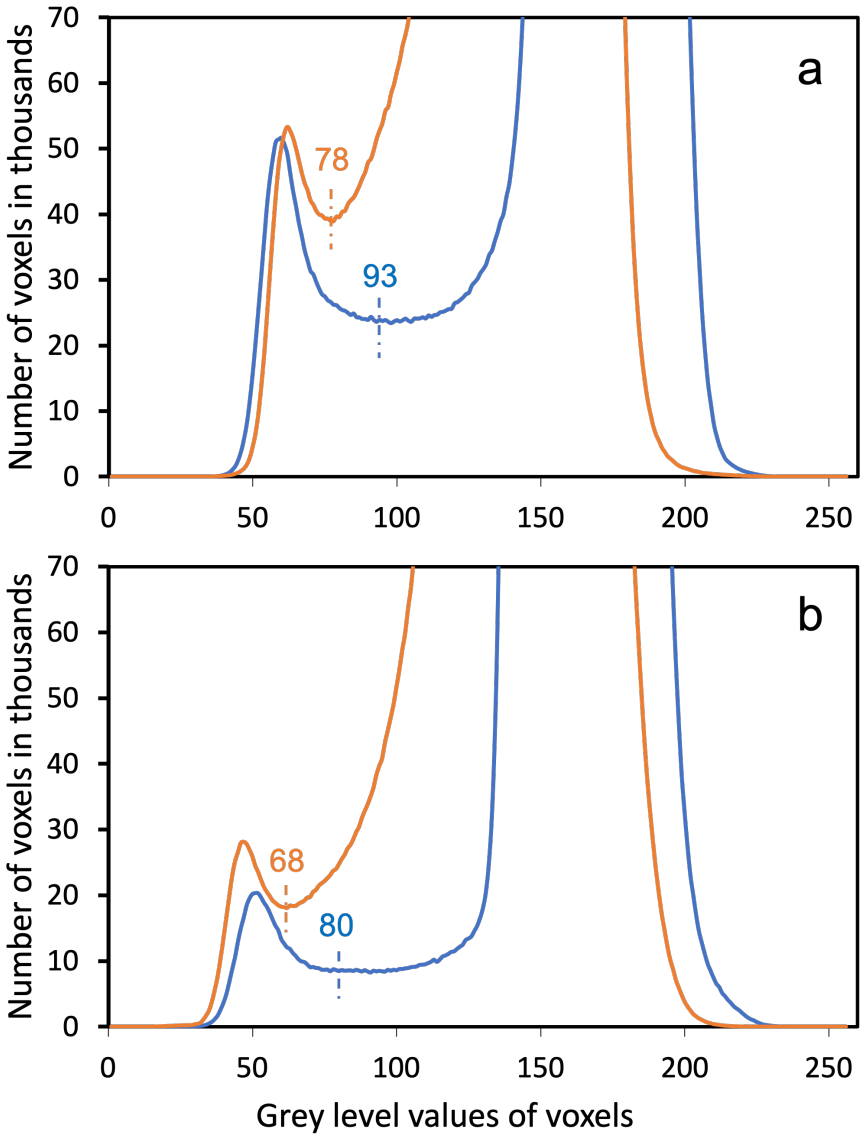

Figure 1 Distribution of the grey level values in the 3D X-ray µ-CT images recorded before freezing (blue) and post-freezing (red) for sample A (**a**) and sample B (**b**). The grey level values corresponding to the threshold value between the air-filled pores and the water saturated porous organic matrix are also plotted.

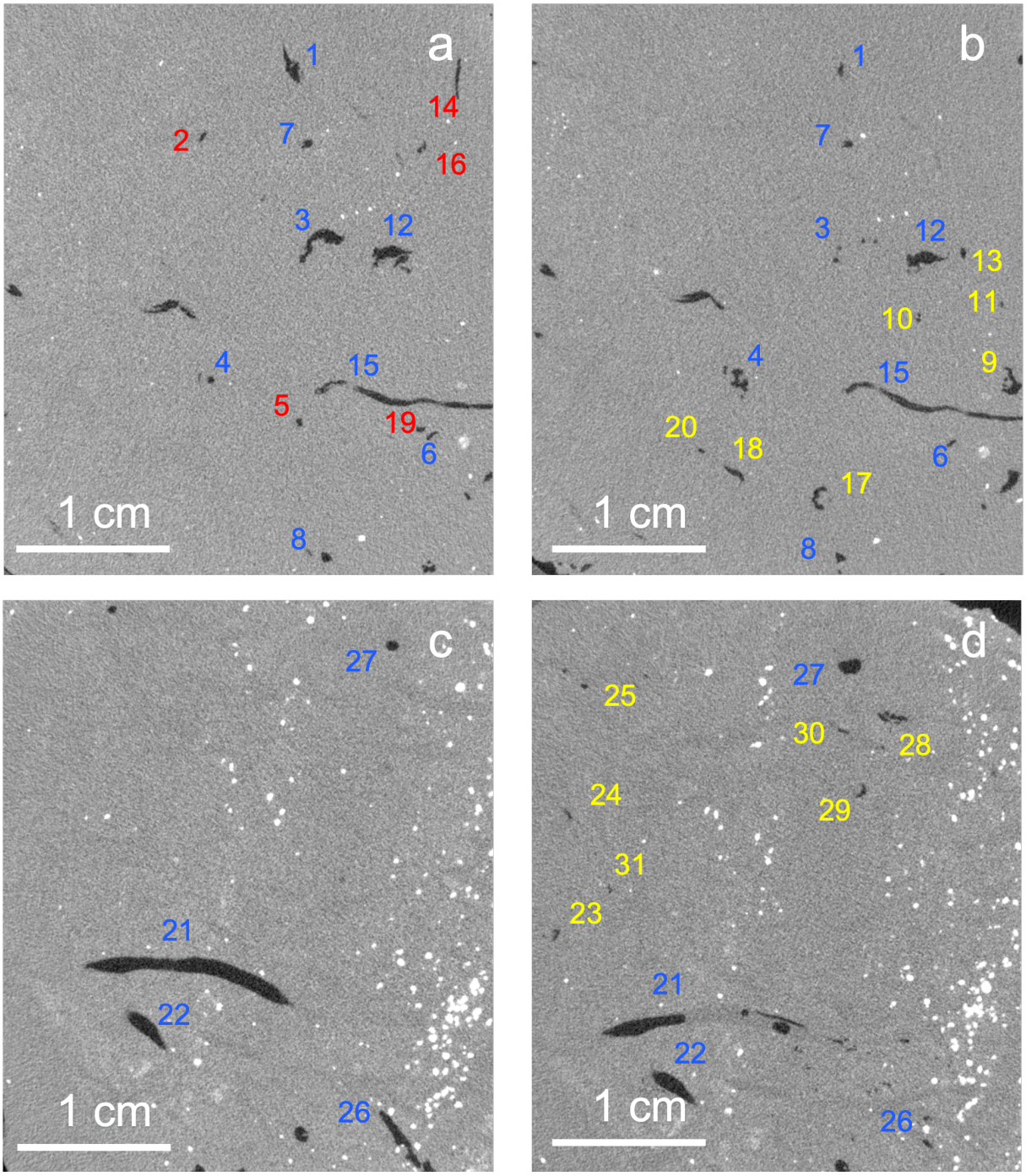

Figure 2. Pairs of 2D µ-CT images of samples A (**a** and **b**) and B (**c** and **d**) extracted from the 3D X-ray µ-CT images in grey levels showing air filled pores (very dark grey), the solid organic material with water filling the associated pores (dark grey) and particles of iron oxy-hydroxides (very light grey). The numbers identify pores which were present before freezing (**a** and **c**) and still present post-defreezing (**b** and **d**) but with a different shape or size (blue), present before freezing and not post-defreezing (red) and not present before freezing but present post-defreezing (yellow).

481

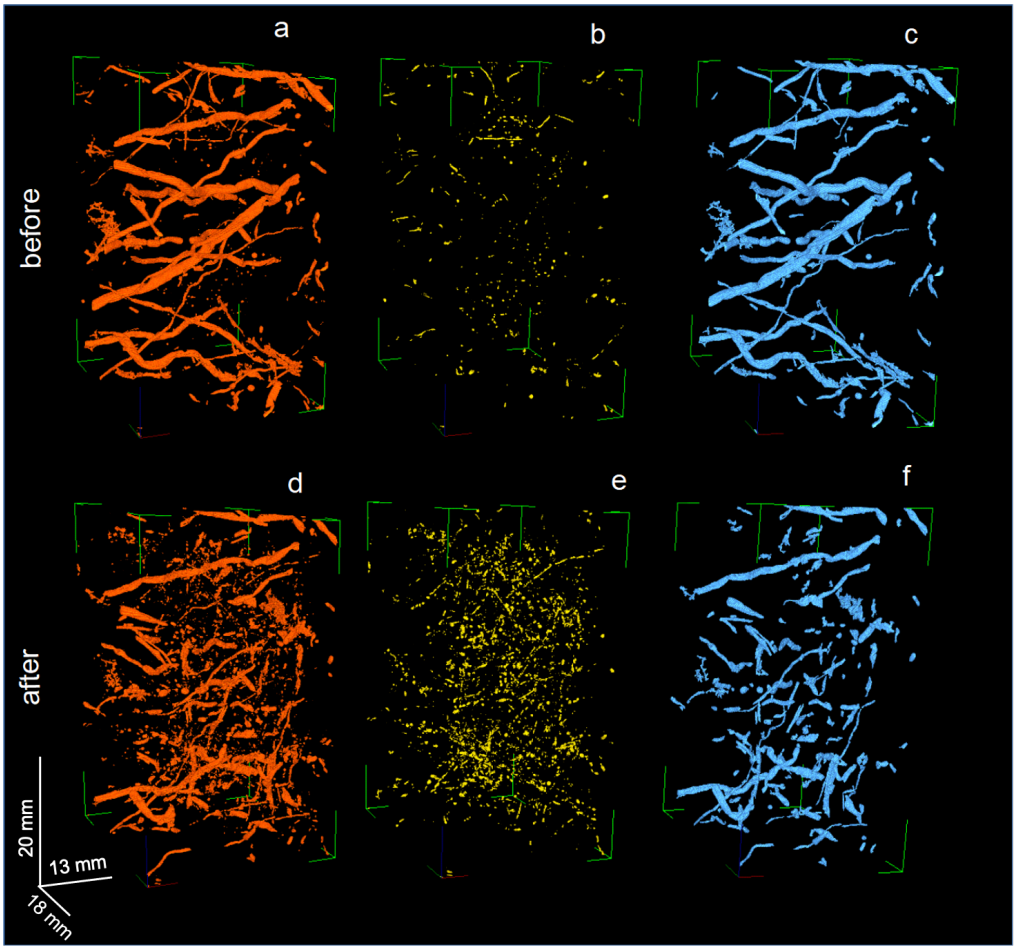

Figure 3. 3D X-ray µ-CT binary images 430×600×800 voxels in volume (~2.6×3.6×4.8 cm^3) of sample A showing the whole pores detected before freezing (**a**) and post-defreezing (**d**), the pores smaller than 500 voxels in volume before freezing (**b**) and post-defreezing (**e**), and the pores larger than 500 voxels in volume before freezing (**c**) and post-defreezing (**f**).

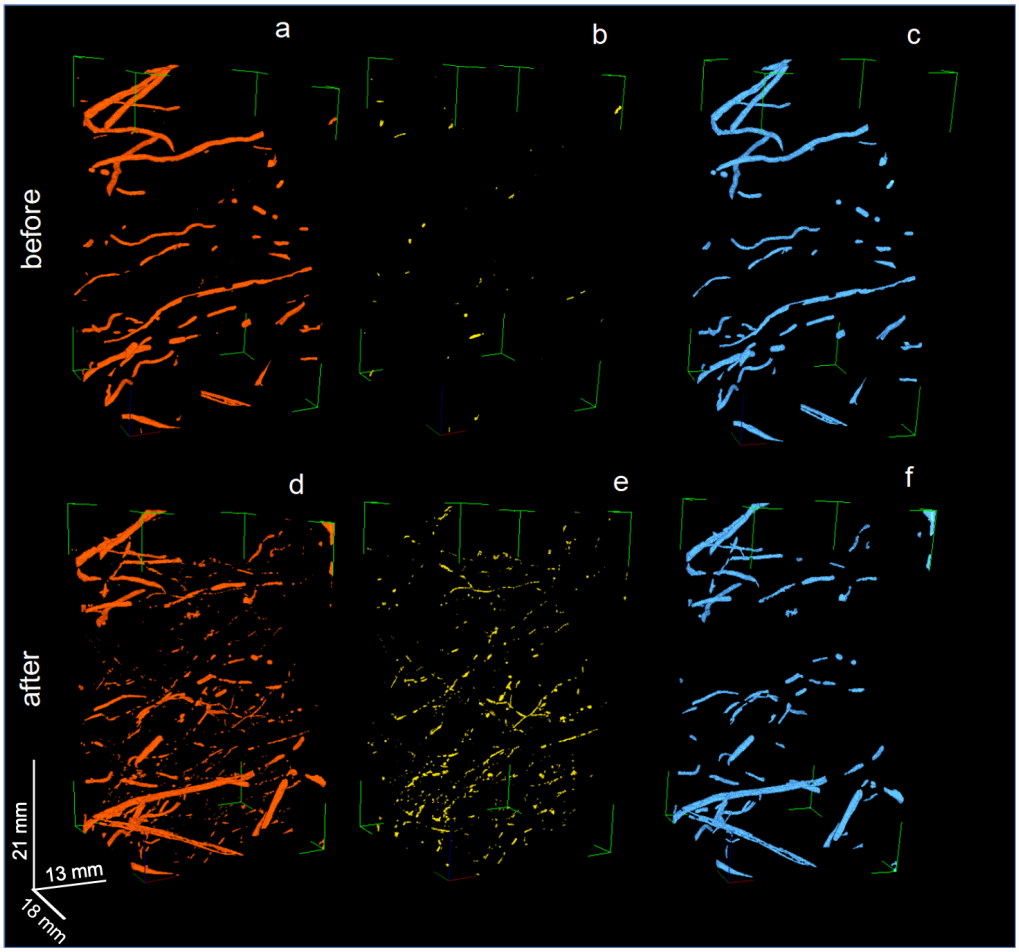

Figure 4. 3D X-ray μ-CT binary images 430×530×850 voxels (~2.6×3.2×5.1 cm^3) of sample B showing the whole pores detected before freezing (**a**) and post-defreezing (**d**), the pores smaller than 500 voxels in volume before freezing (**b**) and post-defreezing (**e**), and the pores larger than 500 voxels in volume before freezing (**c**) and post-defreezing (**f**).

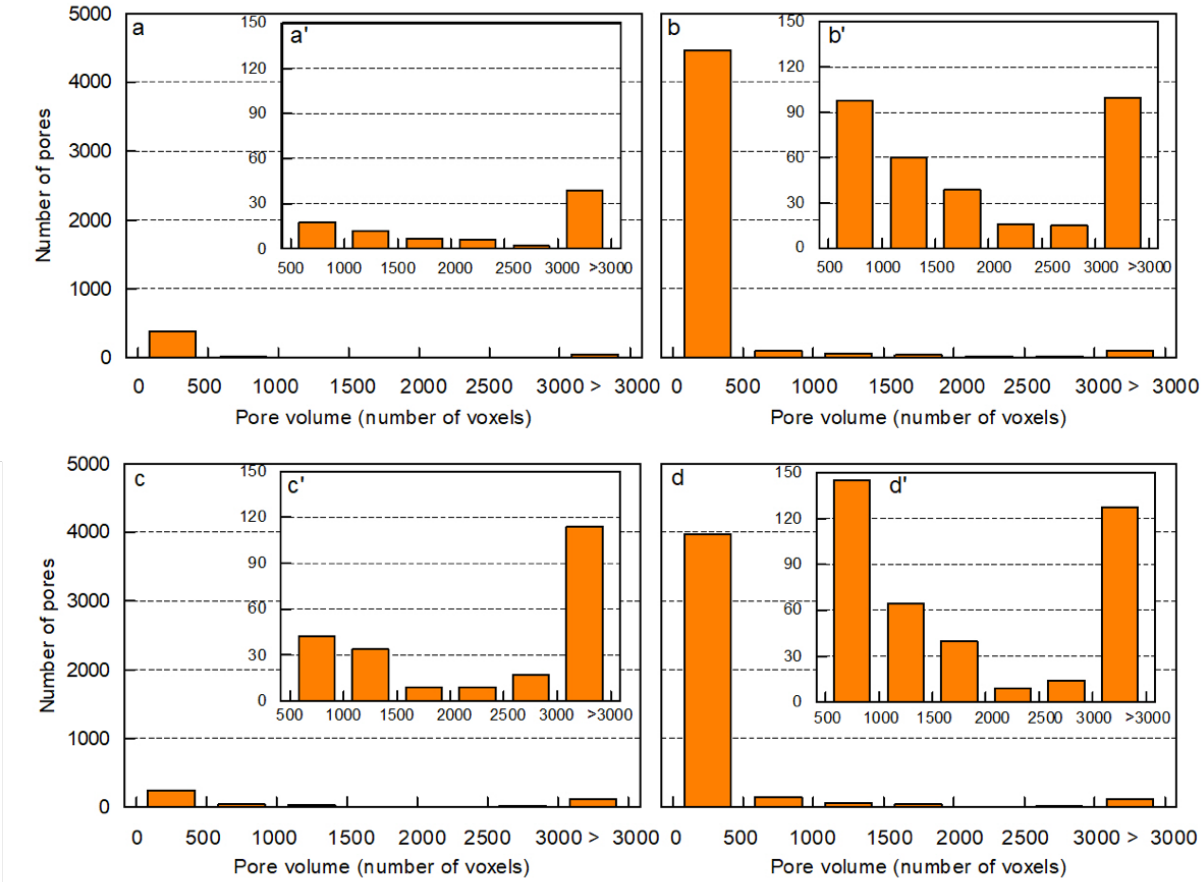

Figure 5. Pore volume distribution according to the number of voxels 60×60×60 µm^3 in volume in the 3D X-ray µ-CT images of sample A before freezing (**a**, **a'**), and post-defreezing (**b**, **b'**), and of sample B before freezing (**c**, **c'**), and post-defreezing (**d**, **d'**).

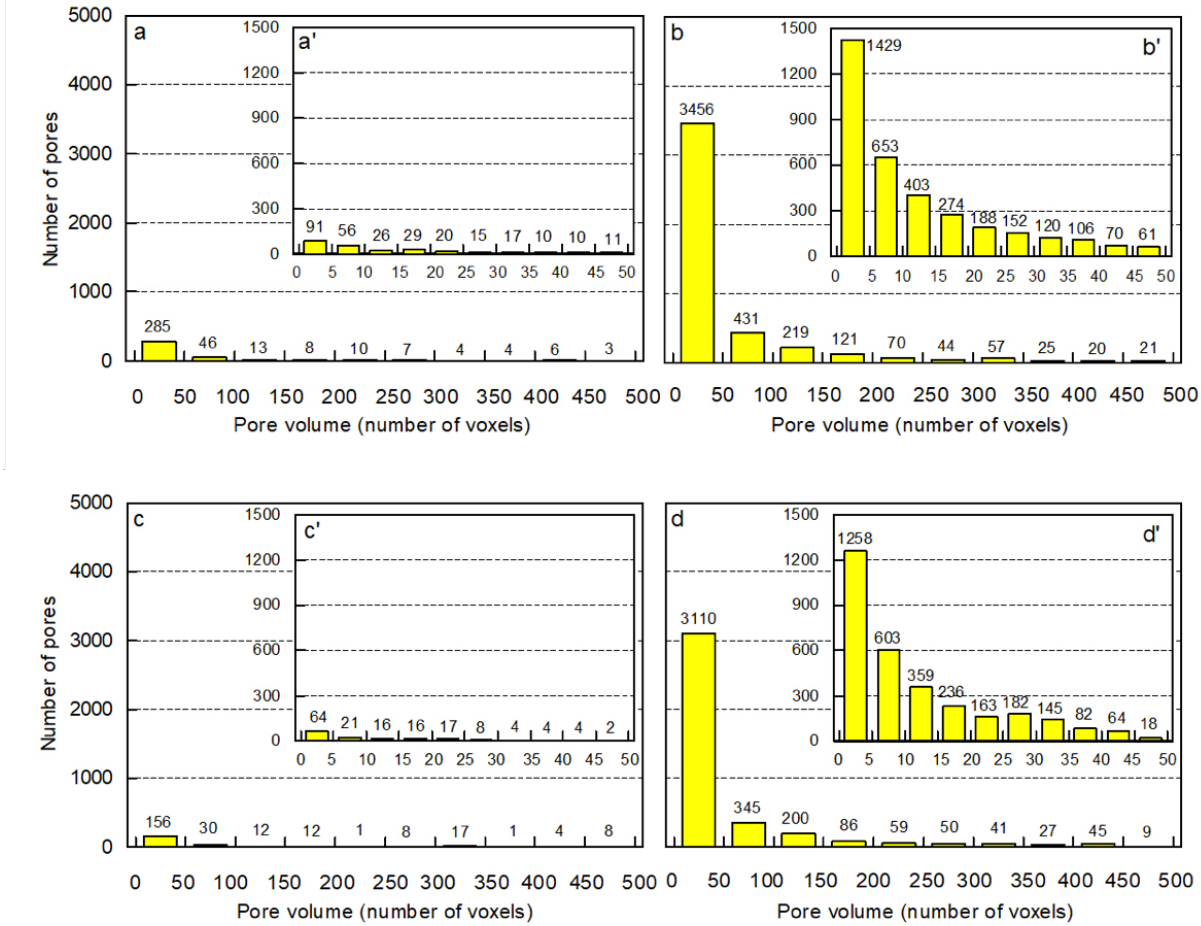

505

506 **Figure 6.** Pore volume distribution according to the number of voxels (≤ 500) and (≤ 50), 60×60×60 μm^3 in volume
507 in the 3D X-ray μ-CT images of sample A before freezing (**a**, **a'**), and post-defreezing (**b**, **b'**), and of sample B
508 before freezing (**c**, **c'**), and post-defreezing (**d**, **d'**).

509

510

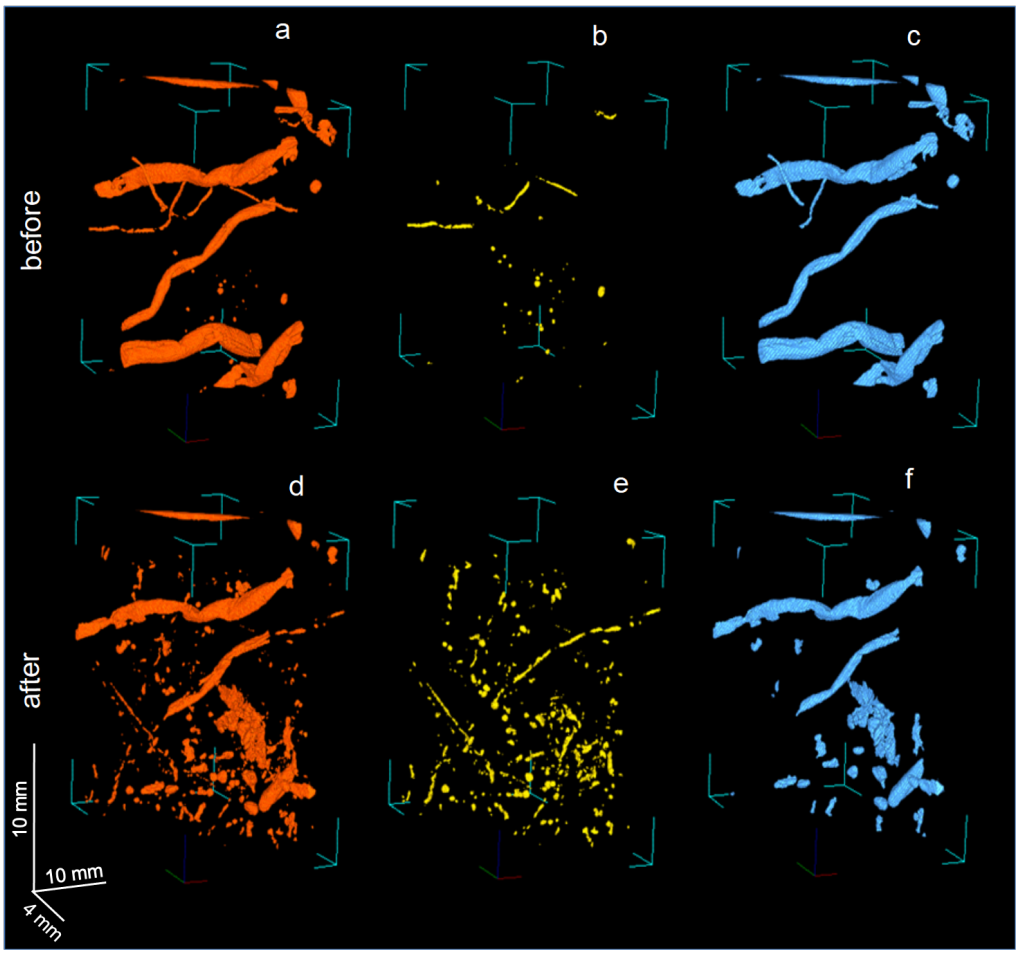

Figure 7. 3D X-ray μ-CT binary sub-images 200×350×350 voxels in volume (~1.2×2.1×2.1 cm^3) of sample A showing all the pores detected before freezing (**a**) and post-defreezing (**d**), the pores smaller than 500 voxels in volume before freezing (**b**) and post-freezing (**e**), and the pores larger than 500 voxels in volume before freezing (**c**) and post-freezing (**f**).

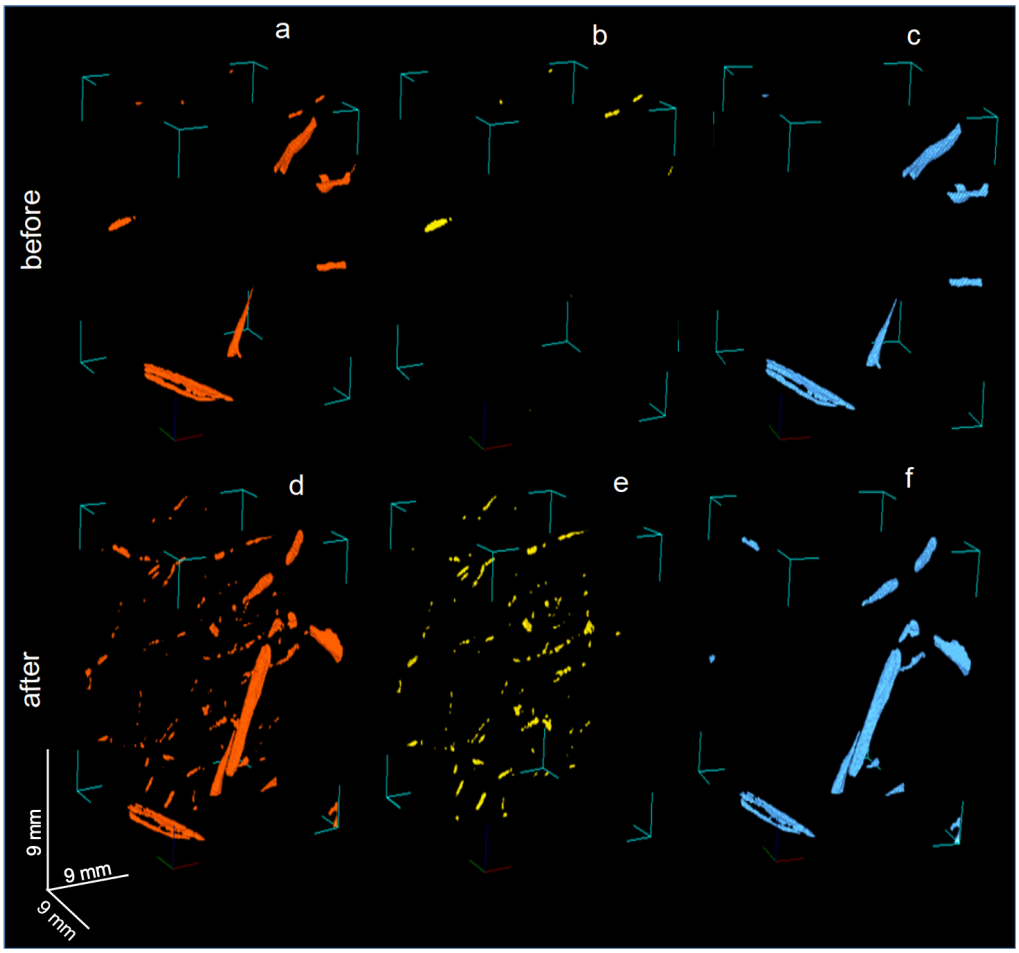

518
519 **Figure 8.** 3D X-ray μ-CT binary sub-images 300×300×300 voxels in volume (~1.8×1.8×1.8 cm^3) of sample B
520 showing all the pores detected before freezing (**a**) and post-frteezing (**d**), the pores smaller than 500 voxels in
521 volume before freezing (**b**) and post-defreezing (**e**), and the pores larger than 500 voxels in volume before freezing
522 (**c**) and post-freezing (**f**).

523

Table 1 Main physical and chemical characteristics of samples A and B of the highly decomposed peat material studied.

Sample	Depth (cm)	ϕ_T	D_p	θ ($cm^3\ cm^{-3}$)	D_b ($g\ cm^3$)	*PPI*	*C:N*
A	25-40	0.918	1.692	0.893	0.135	96.1	12.1
B	25-40	0.904	1.779	0.883	0.178	78.9	16.6

ϕ_T: total porosity, D_p: particle density, θ: water content at sampling, D_b: bulk density and PPI: pyrophosphate index.

Table 2 Characteristics of the pores in the 3D X-ray CT images of samples A and B of the highly decomposed peat material studied before freezing and post-defreezing.

Sample	ϕ	Number of pores	Average size of the pores (voxels)
A before freezing	0.009	470	3952
A post-defreezing	0.017	4792	732
B before freezing	0.005	474	2043
B post-defreezing	0.011	4371	488

ϕ: porosity measured in 3D X-ray CT